Electronic Research Archive

ERA, 33(5): 3135–3157.
DOI: 10.3934/era.2025137
Received: 07 March 2025
Revised: 16 April 2025
Accepted: 08 May 2025
Published: 21 May 2025

http://www.aimspress.com/journal/ERA

Research article

A novel nonlinear viscous contact model with a Newtonian fluid-filled dashpot applied for impact behavior in particle systems

Wanxun Jia[1], Ling Li[1], Haoyan Zhang[1], Gengxiang Wang[1,*] and Yang Liu[2]

[1] School of Mechanical and Electrical Engineering, Xi'an University of Architecture and Technology, Xi'an 710055, China
[2] Exeter Small-Scale Robotics Laboratory, Engineering Department, University of Exeter, Exeter EX4 4QF, UK

* **Correspondence:** Email: wanggengxiang@xauat.edu.cn.

Abstract: In this study, we focused on developing a new viscous contact force model by incorporating a novel viscous fluid damping factor derived from the principles of incompressible Newtonian fluid dynamics. This new viscous fluid damping factor was formulated based on the Navier-Stokes equations, providing a robust framework for accurately modeling energy dissipation during impacts. Building on this foundation, a new coefficient of restitution (CoR) model was proposed by integrating the Hertz contact law with the newly developed viscous fluid damping factor. To validate the correctness of the proposed viscous fluid damping factor, a series of experimental data was collected to examine the relationship between the CoR and the impact velocity. The results confirmed the validity of the proposed CoR model and demonstrated that using fluid-based concepts to describe energy dissipation during impacts between solid bodies is feasible and effective. To highlight the advantages of the new viscous contact model, a comparative analysis was conducted against existing viscous contact models. This comparison demonstrated that the new model achieves the highest accuracy in calculating impact behavior, outperforming conventional models. The superior performance of the new model underscores its potential as a powerful tool for studying dynamic interactions in particle systems. The new viscous contact model was further applied to analyze impact behavior in two scenarios: A bouncing ball and a vertical granular chain. In both cases, the results obtained from the model were validated against experimental data, showcasing its ability to capture complex collision dynamics with remarkable precision. In conclusion, our findings establish the new viscous contact force model as an effective and reliable approach for analyzing impact behavior in particle systems. This investigation paves the way for novel approaches to studying energy dissipation

during impacts in particle systems by utilizing fluid damping factors instead of the internal damping of particles. The proposed contact force model is applicable to a wide range of dynamic systems involving contact interactions. It is particularly effective for simulating contact events in both flexible and rigid multibody systems. Moreover, the model demonstrates strong performance in granular systems, where frequent collisions, adhesion, and nonlinear contact behaviors are prevalent.

Keywords: viscous fluid damping; Navier-Stokes equations; new contact model; CoR model; particle system

1. Introduction

The granular system consisting of large aggregates of discrete particles plays a pivotal role in both industrial applications (such as the pharmaceutical industry [1], chemical industry [2], metal powder technology [3], and agricultural production [4]) and natural processes (such as soil Mechanics, sediment Transport, geological phenomena, and sand wind [5]). These materials exhibit complex behaviors due to the intricate interactions between individual particles and their collective dynamics [6,7]. Moreover, granular materials can exist in solid [8,9], liquid [10], and gaseous states [11], giving rise to unique mechanical properties and intriguing physical phenomena. The frequent occurrence of phase transitions and their associated characteristics significantly influence processing quality and the economic viability of granular operations [12].

Given their critical role, accurately predicting the motion of granular flows is essential for designing more efficient unit operations [13], thereby enhancing throughput and improving product quality [14]. A key challenge in this context lies in understanding the dynamic motion of particles, which is primarily governed by inter-particle collisions [15,16]. Two major approaches have emerged for studying these interactions: Experimental investigations [17,18] and numerical simulations [10,19–21]. Among numerical techniques, one common route treats particle flows as a continuum, applying principles of continuum mechanics in a Eulerian framework [15]. Alternatively, the Discrete Element Method (DEM), originally proposed by Cundall and Strack [22], offers a Lagrangian perspective by modeling particles as individual discrete entities. At present, DEM initially is one of the most frequently used simulation techniques in physics and engineering. In DEM simulations, two dominant contact force models are commonly used. (i) The hard-sphere model, proposed by Alder and Wainwright [23], treats collisions as quasi-instantaneous events. It focuses on calculating post-impact velocities using large time steps, based on momentum conservation during impact. (ii) The soft-sphere model [24], in contrast, resolves the full contact process by accounting for contact force, particle overlap (penetration), and post-impact velocity. This approach requires very small-time steps to accurately capture the short-duration impact events between particles. The soft-sphere model typically includes both linear and nonlinear contact force models, often based on Hertzian contact theory. The linear or nonlinear nature of these models is largely determined by the damping factor, especially when the damping term depends on the relative contact deformation. Several nonlinear contact models, such as the Kuwabara and Kono model [25], Tsuji et al. model [26], and Jankowski model [27], have been proposed to derive more accurate viscous fluid damping factors for energy dissipation during impact. However, these models fall short because their damping formulations do not rigorously account for energy conservation. To address this, some researchers introduced empirical damping values directly

into the models, such as Schwager and Pöschel [28], Lee and Herrmann [29], and Ristow [30]. Yet, these empirical damping factors fail to precisely estimate energy dissipation, as their values are difficult to determine accurately. As a result, the debate over whether a linear or nonlinear damping approach is more appropriate remains unresolved in the DEM research community [11].

Generally, nonlinear viscous fluid damping factors, used to represent energy dissipation during impact, are often derived by approximating linear or nonlinear one-degree-of-freedom vibration systems. These factors are closely related to the material properties of the colliding bodies and the coefficient of restitution (CoR). Beyond this common approach, various other methods have been developed to describe energy dissipation, as a wide range of damping devices have been introduced, such as metal dampers, friction dampers, lead dampers, viscoelastic dampers, and fluid viscous dampers [31,32]. Marshall [33] presented a simple expression for fluid damping due to squeeze-film dynamics, which arise from changes in contact region radius during collisions. His simulations showed that the damping force is highly sensitive to the minimum distance between particle surfaces. Ray and Kempe [11] proposed an efficient approximation for modeling soft-sphere collisions within the Discrete Element Method (DEM) framework in viscous fluids. Their method provides sufficient accuracy while simplifying the governing equations, enabling the calculation of collision time and CoR with fewer parameters and reduced computational cost. Utsumi [34] studied the damping ratio in low-gravity sloshing, considering energy loss due to contact angle hysteresis, using a semi-analytical method for arbitrary axisymmetric tanks. Shi and Polycarpou [35] developed a straightforward experimental method using contact resonance to measure the contact stiffness and damping of Hertzian and rough flat surfaces. This technique relies on analyzing resonance behavior at the contact interface. Fu et al. [36] examined tangential contact stiffness and damping at solid-liquid interfaces under mixed lubrication, showing that their theoretical model closely matched experimental data in both trend and magnitude. Zhang et al. [37] introduced a winding rope fluid viscous damper, which enhances damping through frictional amplification. Their theoretical and experimental results showed strong agreement. Zhang and Turner [38] proposed a linear fluid damping model using beam-type resonators as viscosity and pressure sensors. This model leverages fluid damping effects to monitor changes in environmental viscosity and pressure.

It is worth noting that the viscous fluid damping factor in the contact force model leads to a nonphysical attraction force at the end of the recovery phase. The nonphysical attractive force arises from the fact that the damping force exceeds the elastic force at the end of the recovery phase [20]. Alizadeh et al. [39] introduced an innovative nonlinear contact force model incorporating a dashpot filled with non-Newtonian fluid. This model significantly improves the prediction of the coefficient of restitution (CoR) and effectively reduces the unphysical attraction force observed at the end of a collision. The non-Newtonian fluid enables dynamic adjustment of damping during impact, resulting in a more realistic simulation of collision behavior. Ye and Zeng [40] proposed a normal contact force model with a nonlinear, size-dependent dashpot. Their results showed that this approach effectively mitigates the unphysical tension forces during the recovery phase, enhancing the accuracy of collision dynamics simulations. Poursina and Nikravesh [41] developed an optimization method for calculating an equivalent damping coefficient in a spring-damper system composed of a linear damper and a spring with Hertzian contact force. By assuming particle separation occurs when the contact force reaches zero, their model eliminates the nonphysical attraction force during restitution, improving simulation fidelity. Similarly, Schwager and Pöschel [42] identified that attraction forces stem from the assumption of immediate particle shape recovery upon separation. They introduced revised boundary

conditions, delaying shape recovery until after contact is lost, which removed the unrealistic forces. Ji and Shen [43] also analyzed contact models and confirmed that attraction forces emerge at the end of the recovery phase, affecting granular flow dynamics. Collectively, these studies highlight the adverse impact of attraction forces on post-impact velocity and CoR, often leading to overestimation of particle motion. To address this, we propose an improved viscous fluid damping factor that accurately captures energy dissipation during impact. Additionally, a balance parameter is introduced to eliminate the influence of unphysical attraction forces on post-impact velocity and CoR, thereby enhancing the predictive accuracy of particle flow simulations.

Although the prevailing references tried to establish the damping factors by the dimensionless equation of motion of the colliding particles, the proposed viscous fluid damping factors in the equation of motion of the system suffered from dimensional deficiency [11,39,40]. Unfortunately, they ignored the dimension of the damping coefficient so that the improved damping force in the equation of motion lost its physical meaning. Furthermore, the motion status of the particle in the granular system is not evaluated precisely in spite of the nonphysical attraction force that has been concerned [4,39,40,42,44]. In addition to this, the viscous fluid damping factors are, in general, developed by solving vibration systems. However, these viscous fluid damping factors are incapable of describing the energy dissipation during impact between the particles. Therefore, some scholars made use of the empirical values [29,30,45] to represent the damping coefficient. Nevertheless, the prevailing investigations proved that the previous damping coefficients developed by the two approaches above are incapable of accurately describing the energy dissipation [11].

In allusion to the limitations above, a new viscous fluid damping factor is developed from incompressible Newtonian fluid based on the Navier-Stokes equations. The dynamic viscosity of the fluid is treated as the bulk viscosity of the solid to represent the energy dissipation during solid impact. On this basis, a new viscous contact force model is proposed based on the spring-dashpot model. Subsequently, a new CoR model is developed using this new viscous contact force model, which is validated by experimental data to prove the correctness of the new viscous fluid damping factor. A comparison among existing viscous contact models and the new viscous contact model is implemented to illustrate its advantages. Finally, the new viscous contact force model is successfully applied to calculate impact behavior in the particle systems, which is validated by experimental data as well. This investigation is about the ability to account for complex collision behaviors, which opens the door to broader applications in modeling and analyzing granular systems under various impact conditions.

The structure of this investigation can be organized as follows: In Section 2, a physical spring-dashpot model is established. A new viscous fluid damping factor and a new viscous contact force model are formulated based on the Navier-Stokes equations in Section 3. A new CoR model and its validation are implemented in Section 4. A comparison analysis among the new model and existing viscous models is in Section 5. The application of the new contact force model is validated in the bouncing ball and vertical granular chain in Section 6. The major conclusions are summarized in Section 7.

2. Physical spring-dashpot model incorporating fluid's viscosity

Contact behavior is an inevitable phenomenon in the colliding particle system. It is worthwhile to mention that the contact behavior dissipates the kinetic energy of the particles in the granular system. Precisely evaluating the dissipation energy during impact is crucial to the motion status of the particles

after impact and the prediction of the maximum contact force, which is an important index for judging whether the mechanical structure is damaged by the impact behavior. Moreover, the accurate estimation of impact behavior between the colliding particles facilitates the structure optimization of the mechanical system and improves the production output of the granular system. Accordingly, how to precisely calculate energy loss plays a decisive role in the motion prediction of the colliding particles after impact.

It is well known that the damp factor contributes to dissipating energy during impact. In this section, we propose a new fluid damping factor developed from an incompressible Newtonian fluid. Namely, the fluid damping factor is treated as a fluid dashpot in the spring-dashpot model in Figure 1. The mass of the contact bodies is m_1 and m_2, the contact stiffness coefficient is K, and the damping coefficient is D. The contact behavior is described by the spring-dashpot model that is expressed as

$$F = K\delta^{\alpha} + D\delta^{\gamma}\dot{\delta}^{\beta} \tag{1}$$

where δ is the contact deformation; $\dot{\delta}$ is the relative impact velocity; α, β, and γ are the power exponents depending on the nature properties of the contact behavior. Parameter α determines whether the contact behavior is linear or nonlinear. Parameter β is closely related to the impact velocity during contact, while γ is the power exponent of the deformation in the damping force, which is determined by the dimensional characteristics of the damping force.

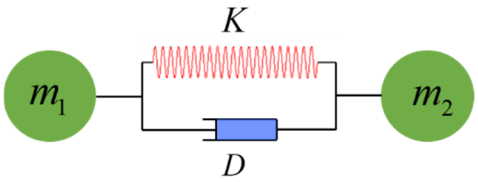

Figure 1. Contact behavior between two particles.

3. Incompressible Newtonian fluid dashpot and the new viscous contact model

The damping factor is crucial in the dissipation of energy in oscillatory systems, such as mechanical, electrical, and structural systems [32]. There are two kinds of damping factors including the hysteresis damping factor and viscous fluid damping factor. Substantially, the damping factor implies the rate at which energy is lost from the system caused by non-conservation forces, such as friction, electromagnetic forces, air resistance, thermal forces, fluid viscosity, etc. In general, the damping factor in the contact force model was developed based on energy conservation or proposed by solving a vibration system. In this section, the non-conservation force is treated as the viscous force from the fluid. Accordingly, a new damping factor caused by the incompressible Newtonian fluid is developed based on the Navier-Stokes equations. Subsequently, we also propose a new contact force model by means of the fluid dashpot in conjunction with the Hertz contact law.

When a small sphere moves through an incompressible Newtonian viscous fluid, the Navier-Stokes equations reduce to the Stokes equation for the low Reynold number flow

$$\begin{cases} \mu\nabla^2\mathbf{u}=\nabla p \\ \nabla\cdot\mathbf{u}=0 \end{cases} \tag{2}$$

where $\mathbf{u}$ is the fluid velocity field; p is the pressure field; and μ is the dynamic viscosity of the fluid (its unit is Pa.s). $\nabla\mathbf{u}$ is the gradient of the velocity field.

To derive the viscous force, there are two boundary conditions: (i) No-slip condition at the sphere's surface, that is, the fluid velocity at the surface of the sphere is equal to the velocity of the sphere. (ii) At infinity, the fluid is undisturbed. When the radius of the fluid velocity field r approaches infinity, the fluid velocity $\mathbf{u}$ approaches zero. Therefore, the Stokes equation in Eq (2) for a sphere moving through a viscous fluid can be solved by means of the boundary conditions. The velocity field around the sphere can be described in polar coordinates (r, θ) regarding the low Reynold number flow

$$\mathbf{u}(r,\theta)=U\left(1-\frac{3R}{2r}+\frac{R^3}{2r^3}\right)\mathbf{e}_r\cos\theta+U\left(1-\frac{3R}{4r}-\frac{3R^3}{4r^3}\right)\mathbf{e}_\theta\sin\theta \tag{3}$$

where θ is the polar angle; r is the polar radius; R is the radius of the sphere; $\mathbf{e}_r$ is the unit vector in the radial direction; $\mathbf{e}_\theta$ is the unit vector in the polar direction.

The pressure field p (r, θ) associated with the fluid is written as

$$p(r,\theta)=\frac{3\mu UR}{2r^2}\cos\theta \tag{4}$$

where U is the velocity of the sphere relative to the fluid.

The stress tensor σ over the sphere's surface is given by

$$\sigma=-p\mathbf{I}+\mu\left(\nabla\mathbf{u}+(\nabla\mathbf{u})^T\right) \tag{5}$$

where $\mathbf{I}$ is the identity tensor.

The drag force on the sphere is evaluated by integrating the stress tensor, which is described as

$$F_d=\int_S\left(-p\mathbf{I}+\mu\left(\nabla\mathbf{u}+(\nabla\mathbf{u})^T\right)\cdot\mathbf{n}\right)dS \tag{6}$$

where $dS=R^2\sin\theta d\theta$ is the differential surface element on the sphere.
where $\mathbf{n}$ is the outward normal to the surface of the sphere, the drag force is solved as [46]

$$F_d=6\pi\mu RU \tag{7}$$

where μ is dynamic viscosity of the fluid (Pa·s or kg/(m·s)).
when the Reynold number Re is greater than 1 and less than 800, a correction factor of the drag force can be written as

$$\phi(Re)=1+0.15Re^{0.687} \tag{8}$$

where Reynold number is expressed as $Re = \frac{R\dot{\delta}}{v_f}$, R is the radius of the sphere, and $v_f = \frac{\mu}{\rho}$ is the kinematic viscosity of the fluid (m²/s).

According to the physical model in Figure 1, U represents the velocity of the sphere relative to the fluid, which can serve as the relative impact velocity $\dot{\delta}$ in the contact behavior. Likewise, the radius of sphere R acts as the relative contact deformation δ because the drag force emanating from the so-called fluid just occurs in the impact behavior. In other words, the drag force is not available when the contact behavior does not happen. Moreover, the viscosity of fluid μ is the contact material's bulk viscosity because there is no natural fluid during impact between the colliding particles. Consequently, Eq (7) can be rewritten as

$$F_d = 6\phi\left(Re\right)\pi\mu\delta\dot{\delta} \tag{9}$$

The fluid dashpot model is expressed as

$$D = 6\phi\left(Re\right)\pi\mu \tag{10}$$

When the fluid dashpot is derived by the Navier-Stokes equations, a new nonlinear viscous contact force model can be formulated based on the Hertz contact law

$$F = K\delta^{\frac{3}{2}} + D\delta\dot{\delta} \Rightarrow F = K\delta^{\frac{3}{2}} + 6\phi\left(Re\right)\pi\mu\delta\dot{\delta} \tag{11}$$

where m is the mass of the contact system $m = m_1 m_2 / \left(m_1 + m_2\right)$; $K\delta^{\alpha}$ is the Hertz contact force, and K is the Hertz contact stiffness coefficient, which is written as

$$K = \frac{4}{3}\left(\frac{1-\nu_i^2}{E_i} + \frac{1-\nu_j^2}{E_j}\right)^{-1}\sqrt{\frac{R_i R_j}{R_i \pm R_j}} \tag{12}$$

where R_i and R_j are the radii of curvature of the contact bodies, E_i and E_j are Young's modulus of the contact bodies, and ν_i and ν_j are the Poisson ratios of the contact material.

4. A new CoR model based on the viscous contact model

Since the coefficient of restitution (CoR) model is closely related to the damping term in the contact force model, we derive a new CoR model based on the new viscous contact force model and energy conservation during impact. To validate the correctness of the new CoR model, we collect a series of experimental data to prove the new CoR model. More importantly, the reasonability of the CoR model provides solid evidence for the new viscous fluid dashpot model and the new viscous contact force model. Therefore, we first derive a new CoR model, which is then validated by experimental data from the metal and nonmetal impact events. On this basis, the new viscous contact force model is also validated by the reference solution and new CoR model.

4.1. Development of a new CoR model

The damping term in the contact force model serves to dissipate kinetic energy during impact. Similarly, in the new viscous contact force model, the fluid dashpot plays the role of dissipating energy. In contrast, the elastic force term functions to store energy, facilitating the separation of the contact bodies after the impact. Regarding energy conservation during the compression phase, we aim to derive a new CoR model based on the new viscous contact force model.

First, the dissipation energy can be estimated by directly integrating the new damping force term in Eq (11)

$$\Delta E = \int_0^{\delta_{\max}} D\delta\dot{\delta} d\delta \tag{13}$$

where $\delta_{\max}$ is the maximum contact deformation.

The impact velocities before and after the collision can be written as

$$\begin{cases} \dot{\delta}_c = \dot{\delta}_0 \sqrt{1-\left(\dfrac{\delta}{\delta_{\max}}\right)^{2.5}} \\ \dot{\delta}_r = \dot{\delta}_f \sqrt{1-\left(\dfrac{\delta}{\delta_{\max}}\right)^{2.5}} \end{cases} \tag{14}$$

where $\dot{\delta}_0$ is the initial impact velocity; $\dot{\delta}_c$ is the impact velocity at the compression phase; $\dot{\delta}_r$ is the impact velocity at the recovery phase; and $\dot{\delta}_f$ is the impact velocity after impact. Based on the definition of Newton's CoR, the relationship between the impact velocities before and after the collision can be expressed as

$$e = -\frac{\dot{\delta}_f}{\dot{\delta}_0} \tag{15}$$

where e is the coefficient of restitution.

Therefore, the total energy loss during impact, including both compression and recovery phases, can be written as

$$\begin{cases} \Delta E_c = \int_0^{\delta_{\max}} D\delta \left|\dot{\delta}_0\right| \sqrt{1-\left(\dfrac{\delta}{\delta_{\max}}\right)^{2.5}} d\delta \\ \Delta E_r = \int_0^{\delta_{\max}} D\delta \left|\dot{\delta}_f\right| \sqrt{1-\left(\dfrac{\delta}{\delta_{\max}}\right)^{2.5}} d\delta \end{cases} \tag{16}$$

The total dissipation energy can be calculated as

$$\begin{aligned} \Delta E &= \Delta E_c + \Delta E_r = \int_0^{\delta_{\max}} D\delta \left|\dot{\delta}_0\right| \sqrt{1-\left(\frac{\delta}{\delta_{\max}}\right)^{2.5}} d\delta + \int_0^{\delta_{\max}} D\delta \left|\dot{\delta}_f\right| \sqrt{1-\left(\frac{\delta}{\delta_{\max}}\right)^{2.5}} d\delta \\ &= AD(1+e)\dot{\delta}_0 \delta_{\max}^2, A = \int_0^1 x\sqrt{1-x^{2.5}}dx \end{aligned} \tag{17}$$

Moreover, the energy loss before and after the collision can be expressed as based on the energy conservation [47]

$$\Delta E = T^{(-)} - T^{(+)} = \frac{1}{2} m\left(1-e^2\right)\dot{\delta}_0^2 \tag{18}$$

where $T^{(-)}$ is the kinetic energy before impact, and $T^{(+)}$ is the kinetic energy after impact.

The fluid dashpot model *D* is derived from the Navier-Stokes equations, which can be used to precisely represent the energy dissipation during impact. Nevertheless, it is emphasized that the proposed fluid dashpot model is used to describe the energy dissipation for the collision behavior between the solid bodies. The dynamic viscosity of the fluid can be treated as the internal damping of the solid contact body, which is equivalent to the CoR for the collision behavior of the colliding particles. Accordingly, combining Eqs (17) and (18), the maximum contact deformation can be expressed as

$$AD\left(1+e\right)\dot{\delta}_0\delta_{\max}^2 = \frac{1}{2} m\left(1-e^2\right)\dot{\delta}_0^2 \Rightarrow \delta_{\max} = \sqrt{\frac{m}{2AD}\left(1-e\right)\dot{\delta}_0} \tag{19}$$

Further, the equation about energy conservation during the compression phase is expressed as

$$\frac{1}{2} m\dot{\delta}_0^2 = \int_0^{\delta_{\max}} K\delta^{1.5} d\delta + \Delta E_c \tag{20}$$

According to Eq (16), the dissipation energy at the compression phase is given by

$$\Delta E_c = \int_0^{\delta_{\max}} D\delta\left|\dot{\delta}_0\right|\sqrt{1-\left(\frac{\delta}{\delta_{\max}}\right)^{2.5}}\, d\delta = AD\dot{\delta}_0\delta_{\max}^2 \tag{21}$$

Combining Eqs (20) and (21),

$$\frac{1}{2} m\dot{\delta}_0^2 = \int_0^{\delta_{\max}} K\delta^{1.5} d\delta + AD\dot{\delta}_0\delta_{\max}^2 \Rightarrow \frac{1}{2} m\dot{\delta}_0^2 = \frac{2}{5} K\delta_{\max}^{2.5} + AD\dot{\delta}_0\delta_{\max}^2 \tag{22}$$

In order to obtain the analytical solution of the CoR, an assumption ($\delta_{\max}^{2.5} = \psi\delta_{\max}^2$) is introduced into Eq (22). The maximum contact deformation can be solved as

$$\frac{1}{2} m\dot{\delta}_0^2 = \frac{2}{5} K\psi\delta_{\max}^2 + AD\dot{\delta}_0\delta_{\max}^2 \Rightarrow \delta_{\max} = \sqrt{\frac{5m\dot{\delta}_0^2}{4K\psi + 10AD\dot{\delta}_0}} \tag{23}$$

where ψ is a length parameter [20], which aims to obtain an analytical solution for the CoR model.

Combining Eqs (19) and (23), the new CoR model can be obtained as

$$\begin{cases} \delta_{\max} = \sqrt{\dfrac{m}{2AD}\left(1-e\right)\dot{\delta}_0} \\ \delta_{\max} = \sqrt{\dfrac{5m\dot{\delta}_0^2}{4K\psi + 10AD\dot{\delta}_0}} \end{cases} \Rightarrow e = 1 - \frac{5AD\dot{\delta}_0}{2K\psi + 5AD\dot{\delta}_0} \tag{24}$$

4.2. Validation of the CoR and viscous fluid dashpot models

To validate the new CoR and new viscous fluid dashpot model, we collect two kinds of experimental data from literature about metal and nonmetal impact events. Here, we aim to prove the correctness of the new CoR model and illustrate the generality of the new viscous fluid dashpot model at the same time. On this basis, we prove the reasonability of the new viscous contact force model according to the reference solutions obtained from the definition of Newton's CoR model. The simulation parameters related to metal material are derived from two separate sets of experimental tests, as shown in Table 1.

Table 1. Contact parameters for the metal materials.

Experiments	Material	R (mm)	ρ (kg/m^3)	E (GPa)	v	μ (Pa.s)
Jackson et al.[48]	Aluminum oxide	2.5	4000	370	0.22	1.5E5
	Steel	∞	——	200	0.29	——

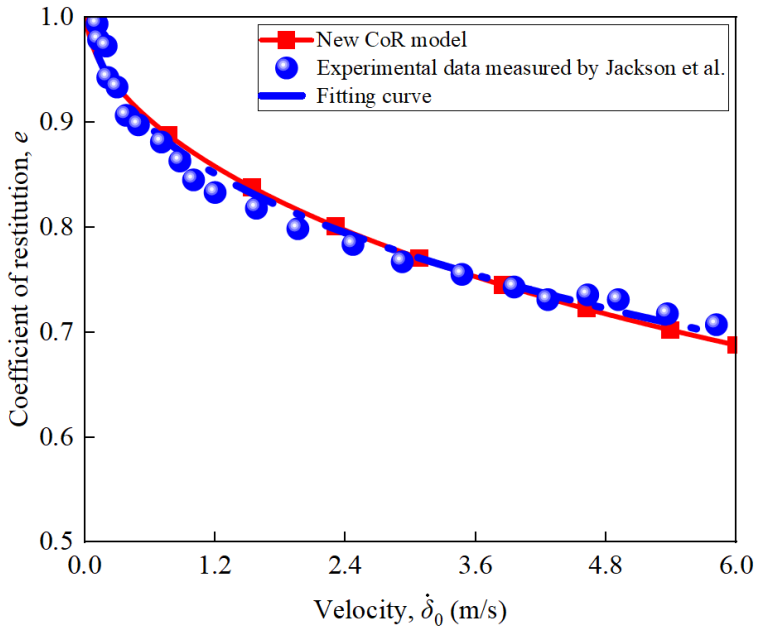

Figure 2. Comparison between the experimental data from Jackson et al. and the new CoR model.

In Figure 2, the new CoR model is almost the same as the fitting curve generated by the experimental data, which adequately proves the reasonability of the new CoR model. Further, the new viscous dashpot model is also validated by this comparison analysis. This conclusion illustrates the new viscous dashpot model is capable of describing energy dissipation during impact. More importantly, the conclusion drawn from this comparative analysis indirectly demonstrates that the new viscous contact model can accurately describe the collision process between particles, particularly the post-impact velocity. It is worth noting that the post-impact velocity can be determined in advance according to the definition of Newton's CoR model when the initial impact velocity and CoR are known.

Table 2. The error between the reference solution and post-impact velocity based on Jackson et al. experiments.

$\dot{\delta}_0$ (m/s)	e	$\dot{\delta}_{f_0}$ (m/s)	$\dot{\delta}_f$ (m/s)	$\frac{\lvert\dot{\delta}_f - \dot{\delta}_{f_0}\rvert}{\dot{\delta}_{f_0}} \times 100\%$
0.1	0.9679	0.0968	0.0967	0.0418%
0.5	0.9181	0.4591	0.4590	0.0028%
1.0	0.8800	0.8800	0.8799	0.0159%
1.5	0.8510	1.2765	1.2760	0.0360%
2.0	0.8270	1.6540	1.6529	0.0689%
2.5	0.8062	2.0155	2.0135	0.0997%
3.0	0.7877	2.3631	2.3601	0.1274%
4.0	0.7559	3.0236	3.0173	0.2094%
5.0	0.7289	3.6445	3.6336	0.2988%
6.0	0.7054	4.2324	4.2153	0.4031%

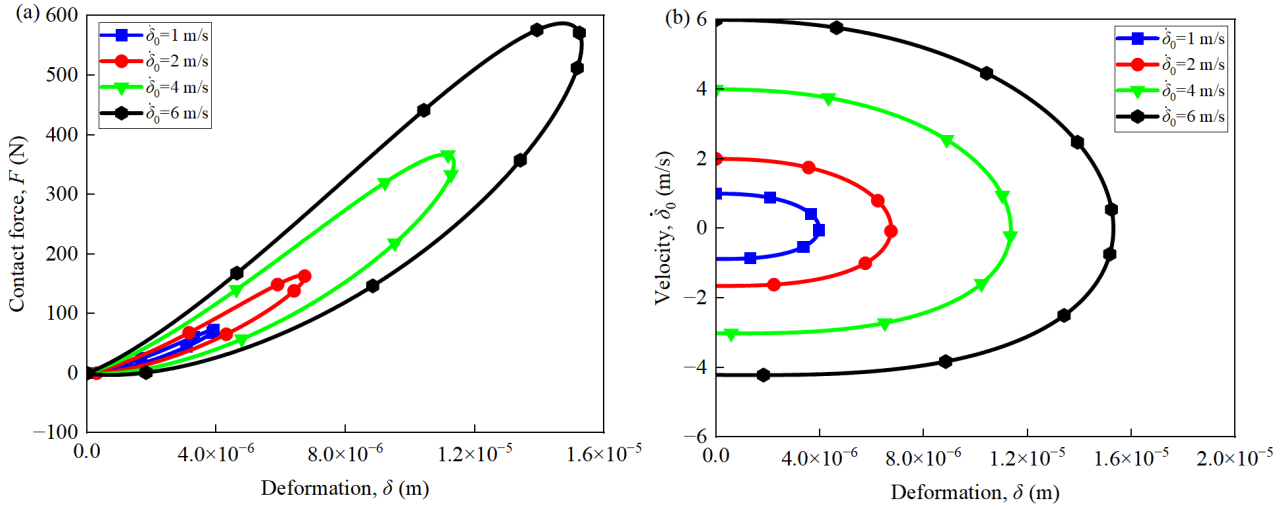

Figure 3. Dynamic responses of the new viscous contact model using Jackson et al. experimental parameters.

Table 2 provides a series of the initial impact velocity. Furthermore, the CoR value can be calculated based on the new CoR model. Therefore, the reference solution of the post-impact velocity can be confirmed, too. They can serve as reference solutions to validate the accuracy of the new viscous contact force model. The post-impact velocity in Table 2 is calculated based on the new viscous contact force model. The error percentage between the post-impact velocity and post-impact velocity does not exceed 1% under different initial impact velocities, which proves that the new viscous contact force model possesses high accuracy when evaluating the impact behavior. The relationships between the contact force and contact deformation are displayed in Figure 3(a) when the initial impact velocity is equal to 1, 2, 3, and 4 m/s, respectively. The relationships between the impact velocity and contact deformation in the case of different initial impact velocities are displayed in Figure 3(b). The dynamic responses in Figure 3 obtained from the new viscous contact force model showcase a reasonable impact process. The greater the impact velocity is, the greater the contact force generated. Likewise, the larger

the impact velocity is, the larger the contact deformation produced. The post-impact velocities in Figure 3(b) can be found in Table 2 when the initial impact velocity is discrepant, which demonstrates that the new viscous contact force model possesses higher accuracy in simulating collision behavior. Table 3 provides material properties of the nonmetal, and Horabik et al. measured the relationship between the CoR and impact velocity in Figure 4.

Table 3. Contact parameters for the nonmetal materials.

Experiments	Material	R (mm)	ρ (kg/m^3)	E (GPa)	v	μ (Pa.s)
Horabik et al. [49]	Rapeseed	0.96	1020	0.065	0.24	3.1E2
	Marble	∞	——	71	0.3	——

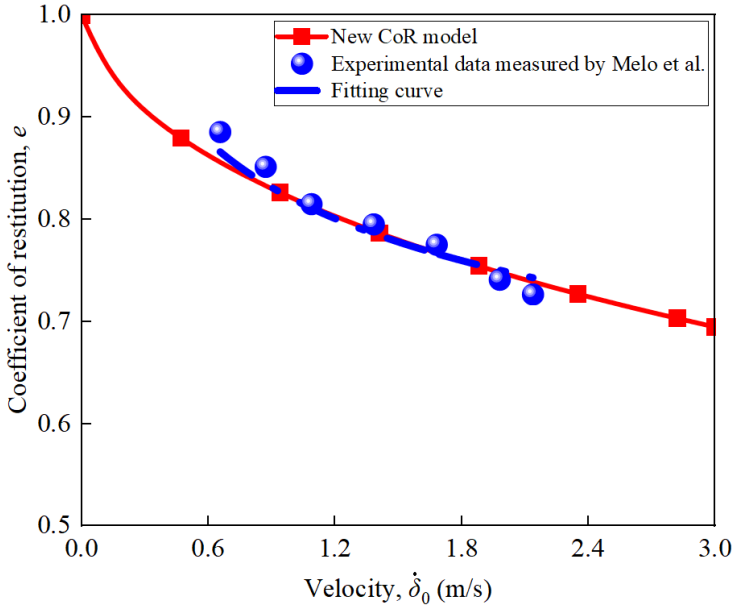

Figure 4. Comparison between the experimental data from Horabik et al. and the new CoR model.

Table 4. The error between the reference solution and post-impact velocity based on Horabik et al. experiments.

$\dot{\delta}_0$ (m/s)	e	$\dot{\delta}_{f_0}$ (m/s)	$\dot{\delta}_f$ (m/s)	$\frac{\lvert\dot{\delta}_f-\dot{\delta}_{f_0}\rvert}{\dot{\delta}_{f_0}}\times 100\%$
0.1	0.9576	0.0958	0.0950	0.8372%
0.4	0.8899	0.3560	0.3560	0.0022%
0.6	0.8628	0.5177	0.5177	0.0050%
0.8	0.8403	0.6722	0.6722	0.0042%
1.0	0.8206	0.8206	0.8206	0.0030%
1.2	0.8031	0.9637	0.9637	0.0017%
1.4	0.7873	1.1022	1.1021	0.0073%
1.6	0.7728	1.2365	1.2363	0.0162%
1.8	0.7595	1.3671	1.3666	0.0402%
2.0	0.7470	1.4940	1.4933	0.0502%

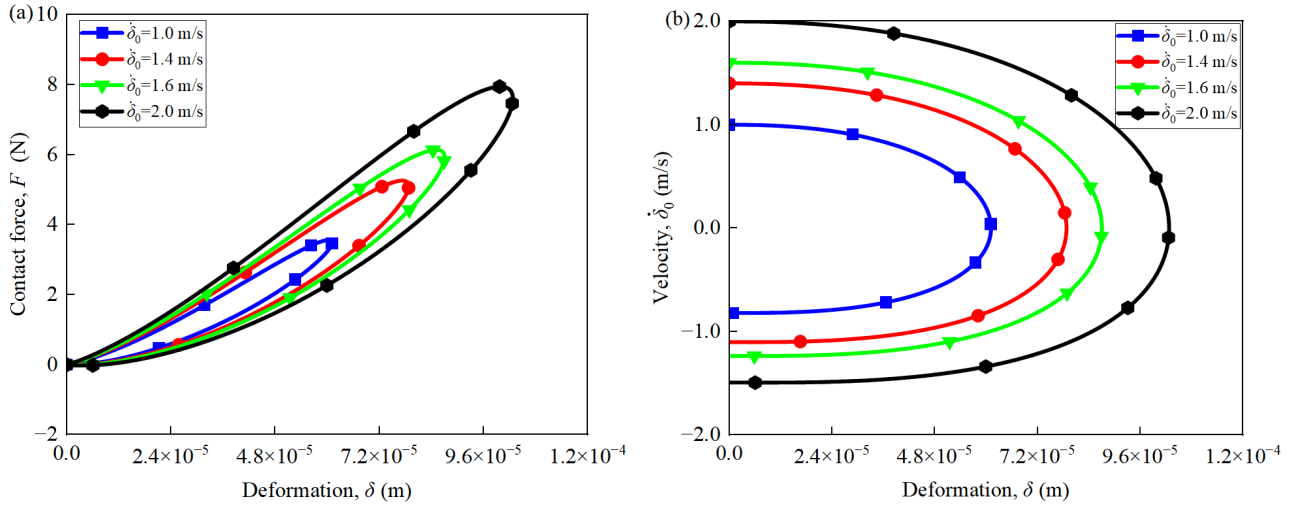

Figure 5. Dynamic responses of the new viscous contact model using Horabik et al.'s experimental parameters.

The new CoR model agrees with the fitting curve obtained by the experimental data, even if the contact material changes from metal in Figure 2 to nonmetal in Figure 4. This conclusion confirms that the new fluid dashpot model is effective in representing energy dissipation during impacts involving non-metal materials. Likewise, Table 4 provides the reference solutions to validate the accuracy of the new contact force model. The error percentage between the reference solution and post-impact velocity under the dissimilar impact velocities is less than 1%. The dynamic responses obtained from the new contact force model can be seen in Figure 5. Since the contact material is nonmetal, the contact deformation in Figure 3 is significantly larger than that in Figure 5, even though the impact velocity in Table 4 is smaller than that in Table 2. These simulation conclusions justify that the new viscous contact force model is reasonable in simulating the non-metal impact behavior.

In this section, we present two types of contact materials to validate the new CoR model using experimental data. The effectiveness of the new viscous fluid dashpot model is also demonstrated through experimental validation of the CoR model, confirming its capability to describe energy dissipation during impact. More importantly, the high accuracy and robustness of the new viscous contact force model are validated using experimental CoR data in conjunction with reference solutions. The model is shown to effectively estimate impact behavior for both metallic and nonmetallic materials. It is worth emphasizing that the new viscous contact force model does not explicitly incorporate the CoR parameter into the fluid dashpot. However, this does not hinder the fluid dashpot's ability to describe energy dissipation during the collision process.

Notably, the dynamic viscosity coefficient μ of the fluid can serve as an equivalent to the CoR within the fluid dashpot, regulating the magnitude of energy dissipation during impact. This highlights the advantages of using μ to describe energy dissipation and supports the validity of the investigation's approach employing an incompressible Newtonian fluid to model energy dissipation in particle collisions. From a fluid dynamics perspective, energy dissipation during collisions between solids can also be effectively described, opening new avenues for extending this concept. The bulk viscosity of the solid is equivalent to the dynamic viscosity coefficient μ of the fluid. Specifically, any physical quantity capable of representing energy dissipation and exhibiting damping characteristics

can be incorporated into contact force models to accurately simulate energy dissipation in particle collision processes.

5. Comparison of the new model with existing viscous models

Once the reasonability of the new contact model has been validated, its advantages should be highlighted by comparing the existing viscous contact force models, including the Kuwabara and Kono (KK) model [25], Tsuji et al. (TS) model [26], Jankowski (JA) model [27], and Lichtensteiger (LI) model [50]. The mathematical formulations of each model can be seen in Table 5.

Table 5. The existing viscous contact force models.

Viscous models	Mathematical formulations
KK model [25]	$F_k = K\delta^{\frac{3}{2}} + \chi_k\delta^{\frac{1}{2}}\dot{\delta}, \chi_k = \frac{3}{2}AK, A = \frac{\gamma_1 D_1 + \gamma_2 D_2}{D_1 + D_2}, \gamma_i = \frac{1}{E_i}\left(\frac{1+v_i}{1-v_i}\right)\left[\frac{4}{3}\eta_{s(i)}\left(1-v_i+v_i^2\right)+\eta_{b(i)}\left(1-2v_i\right)\right.$ ($D_i = \left(1-v_i^2\right)/E_i$ (i = 1, 2 represents the contact bodies); $\eta_{s(i)}$ is the shear viscosity; $\eta_{b(i)}$ is the bulk viscosity; χ_k is the viscous fluid damping factor; E_i is the Young's modulus of the contact bodies; v_i is the Poisson's ratio of the contact bodies.)
TS model [26]	$F_{ts} = K_h\delta^{\frac{3}{2}} + \chi_{ts}\delta^{\frac{1}{4}}\dot{\delta}, \chi_{ts} = \sqrt{5}\left\|\ln e\right\|\sqrt{\frac{K_h M}{\pi^2 + \ln^2 e}}$ (K_h is the Hertz contact stiffness coefficient; χ_{ts} is the viscous fluid damping factor; e is the CoR; M is the equivalent mass of the contact bodies)
JA model [27]	$F_{ja} = K_h\delta^{\frac{3}{2}} + \chi_{ja}\delta^{\frac{1}{4}}\dot{\delta}, \chi_{ja} = 9\sqrt{5}\frac{1-e^2}{e\left[e\left(9\pi-16\right)+16\right]}\sqrt{K_h M}$ (K_h is the Hertz contact stiffness coefficient; χ_{ja} is the viscous fluid damping factor; e is the CoR; M is the equivalent mass of the contact bodies)
LI model [50]	$F = K_h\delta^{\frac{3}{2}} + \chi_{li}\delta\dot{\delta}, \chi_{li} = \frac{\sqrt{5}\left\|\ln e\right\|}{\sqrt{\ln^2 e + \pi^2}}\frac{K_h{}^{4/5}M^{1/5}}{\dot{\delta}_0{}^{3/5}}$ (K_h is Hertz contact stiffness coefficient; χ_{li} is the viscous damping factor; e is the CoR; M is the equivalent mans of the contact bodies)

A systematic comparison analysis between the new contact model and the existing contact model is implemented in this section, which aims to showcase the excellent dynamic performance in calculating the impact behavior of the colliding particles. The simulation parameters are displayed in Table 1. The initial impact velocity is equal to 0.5 m/s, the CoR is calculated as 0.9181 according to the new CoR model in Eq (24). The reference solution of the post impact velocity is equal to 0.4591 m/s in Table 2 based on the definition of Newton's CoR, which is used to rate which viscous contact model is the most accurate one. The post impact velocities obtained from the five dissimilar kinds of

the viscous contact model are displayed in Table 6. The error between the post impact velocity and the reference solution can be seen in Table 6 for each viscous contact model.

Table 6. Error analysis between viscous contact force models and reference solution.

Contact models	$\dot{\delta}_0$ (m/s)	e	$\dot{\delta}_f$ (m/s)	$\frac{\lvert\dot{\delta}_f-\dot{\delta}_{f_0}\rvert}{\dot{\delta}_{f_0}}\times 100\%$
New model	0.5	0.9181	0.459037	0.0028%
TS model	0.5	0.9181	0.459064	0.0030%
JA model	0.5	0.9181	0.418624	8.8064%
KK model	0.5	0.9181	0.301940	34.2250%
LI model	0.5	0.9181	0.307863	32.9348%

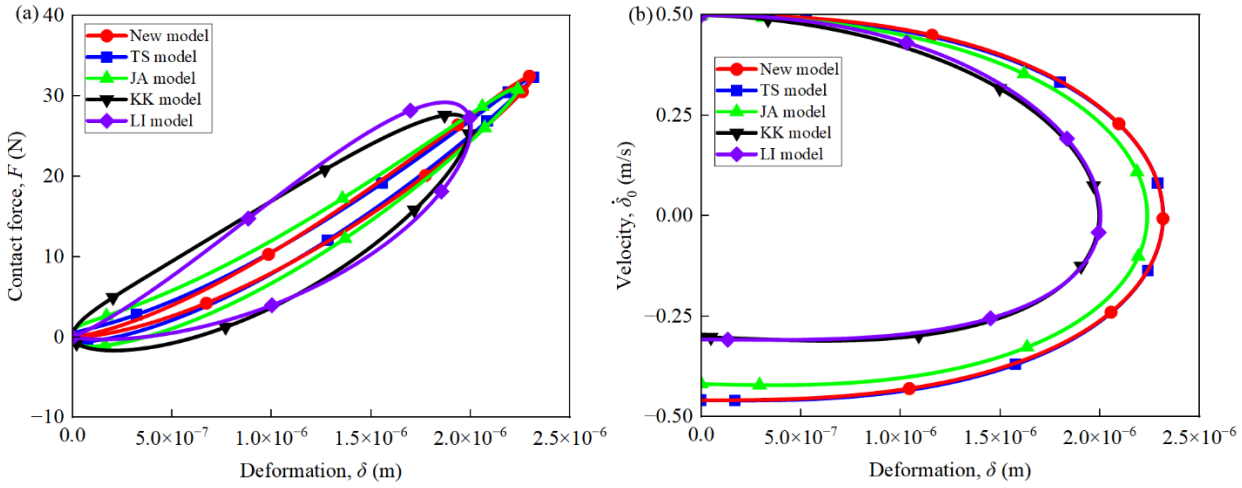

Figure 6. Comparison among the existing viscous contact model and new viscous contact model.

The newly developed viscous contact model demonstrates superior accuracy compared to all viscous contact models, and it is almost the same as the TS model, which is widely regarded as the most precise among the existing viscous contact models [19]. In terms of the contact force, the new model closely aligns with the JA and TS models, as illustrated in Figure 6(a), highlighting its consistency with previously established approaches. On the other hand, the KK and LI models exhibit significant energy dissipation discrepancies and dissipate more energy observed in Figure 6(a). This excessive energy dissipation results in post-impact velocities, presented in Figure 6(b), that deviate substantially from the reference solution. Thereby, they fail to provide accurate predictions. In contrast, the new viscous contact model not only accurately captures the maximum contact force but also can accurately calculate the post-impact velocity. This conclusion demonstrates that the new viscous contact model outperforms all existing viscous contact models in accurately estimating the maximum contact force and establishes it as a more reliable and precise approach in contact dynamics modeling.

6. Application of the new viscous contact model in colliding particle systems

The data and model in Section 4 belong to the theoretical analysis of the new contact force model. In this section, we attempt to apply the new contact model for evaluating the particle systems, including

the bouncing ball and vertical granular chain. We aim to prove the practicability of the new contact force model by comparing its simulation results to the experimental data.

6.1. Bouncing ball

A classical bouncing ball example is shown in Figure 7. The experiments involve tracking the trajectory of a solid sphere as it falls with an initial impact velocity of 0.54 m/s onto a solid wall. The ball has a radius of 3 mm. Its initial height above the ground is 0.04 m. No apparent rotation is observed in these devices during the release of the sphere. The spheres are held in place by suction at the tip of a small tube where a reduced pressure is generated by a micropump. The detailed experimental setup can be referred to in the literature [51]. When the contact behavior in the bouncing ball example is modeled as an elastic collision, energy dissipation is considered only due to the transmission of seismic waves. To evaluate the proposed contact model's practicability in handling collision behavior in particle systems, the material of the ball is Teflon, its Young's modulus is 0.4 GPa, Poisson's ratio is 0.46, and the density is 2150 kg/m^3. The bulk viscosity of stainless steel is 3.4×10^3 Pa.s; however, when the number of collisions exceeds 5, it becomes 5.0×10^3 Pa.s to dissipate more kinetic energy of the ball. The plate is made of glass, its Young's modulus is 60 GPa, Poisson's ratio is 0.24, its density is 2500 kg/m^3, and its thickness is 12 mm.

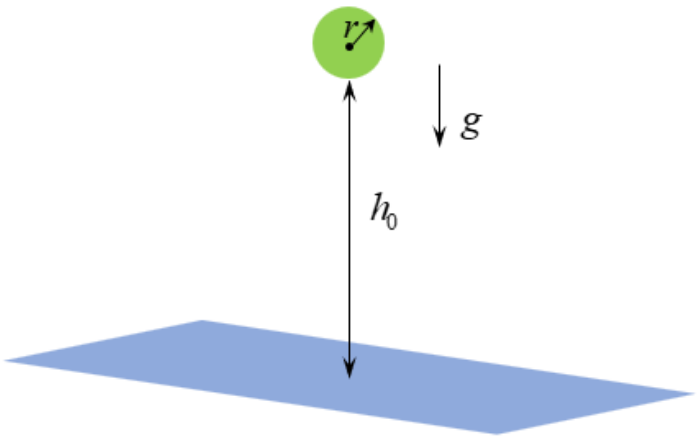

Figure 7. Bouncing ball.

Remarkably, the displacement of the ball shown in Figure 8(a), as calculated using the new contact force model, aligns closely with the experimental data. This consistency demonstrates the model's ability to accurately estimate the impact behavior between the ball and the ground. Such agreement validates the reliability and accuracy of the new contact force model in capturing the key dynamics of collision events. More importantly, this finding supports the feasibility of employing the fluid concept to describe energy dissipation during solid impact events.

The bulk viscosity of a solid can effectively be interpreted as equivalent to the dynamic viscosity of a fluid, reinforcing the idea that fluid-based concepts can be successfully extended to the modeling of solid impacts. This innovative perspective opens new possibilities for understanding and simulating energy dissipation in complex collision scenarios. Furthermore, as shown in Figure 8(b), the velocity of the ball post-impact also matches well with the experimental data. This highlights the capability of

the new viscous contact force model to not only accurately capture the displacement characteristics during the impact process but also precisely determine the post-impact velocity. By accurately describing both the displacement and velocity dynamics, the model demonstrates its robustness and comprehensive applicability in representing the physical phenomena of impact behavior.

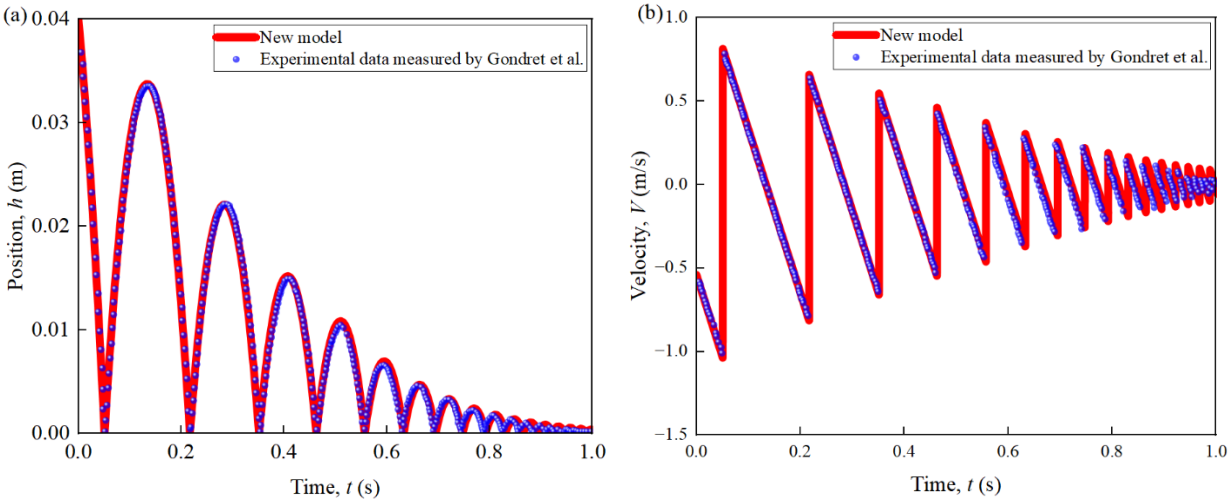

Figure 8. Dynamic responses of the bouncing ball.

6.2. Vertical granular chain

The experimental setup in Figure 9 illustrates a one-dimensional vertical granular chain [52]. The chain is composed of 21 identical stainless-steel particles, excluding the magnetic steel ball. Both chains are positioned on a red brass plate equipped with a piezoelectric sensor to measure the force exerted on the base. Additionally, two piezoelectric sensors are embedded in particles 13 and 17 (counting from the top of the chain, not including the striker). Nonlinear solitary waves are initiated by the impact of alumina (Al_2O_3) cylindrical strikers on the topmost particle of the chain. The detailed structure of this system can be found in references [53,54]. The magnetic steel ball used in the setup has a radius of 2.5 mm and a mass of 0.5115 g, while the grain has a radius of 2.38 mm. The material properties are summarized in Table 7. The particle mass is 0.47 g, and the magnetic force is set to 0. The striker velocity is 0.44 m/s. This experiment investigates the propagation of solitary waves under different contact conditions. The simulation runs for a total time of 400 μs with a time step of 0.03 μs. The bulk viscosity of stainless steel is 1.25×10^5 Pa.s. The integration is performed using MATLAB's builtin Ode45 solver.

Table 7. Material parameters.

Material	Young's modulus	Poisson's ratio	Yield stress
Stainless steel 316	193 GPa	0.300	940 MPa
Red brass	115 GPa	0.307	250 MPa
Al_2O_3 aluminum	416 GPa	0.231	500 Mpa

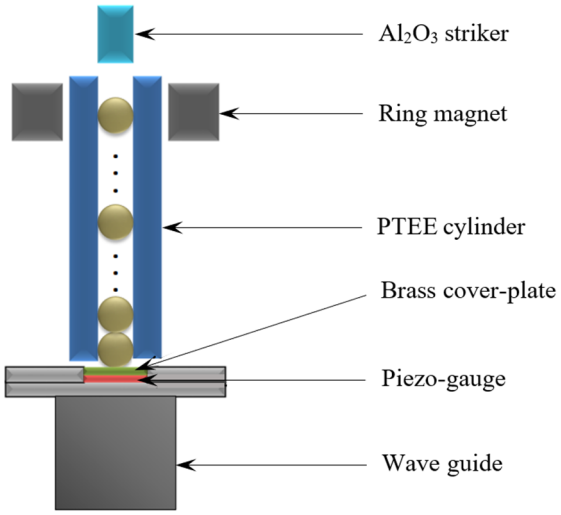

Figure 9. The experimental setup of the vertical granular chain [52].

To observe the solitary waves shown in Figure 10, the contact force values for the 13th particle and the base were shifted along the Y-axis by 25 N and -30 N, respectively. In the first curve, the contact force acting on the 13th particle propagates as a solitary wave along the vertical granular chain. Similarly, the curve for the 17th particle exhibits a comparable propagation pattern. However, the peak values in the 17th particle's curve are spaced closer together, reflecting the increased frequency of contact interactions as the particles approach the base of the chain. When the solitary wave reaches the base, it is reflected back, generating a rebound wave illustrated in the third curve of Figure 10. This reflected wave underscores the base's function in redirecting the energy of the incoming solitary wave.

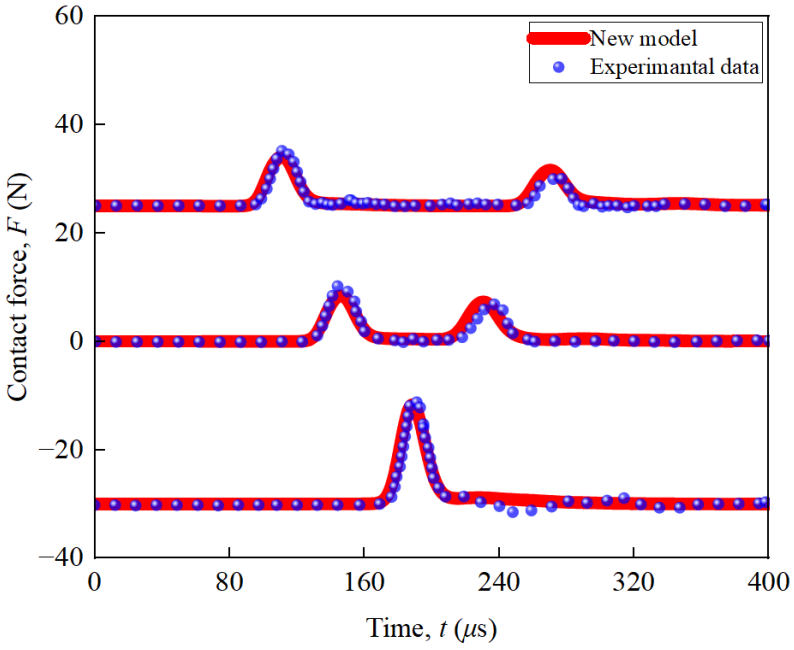

Figure 10. Soliton wave propagation in the vertical granular chain.

Remarkably, the solitary wave propagation calculated using the new viscous contact force model aligns closely with the experimental data, regardless of the specific particle analyzed. This agreement demonstrates the model's robustness and accuracy in capturing the dynamics of granular chain collisions. Furthermore, the new viscous contact force model successfully evaluates not only the impact behavior of individual colliding particles but also the complex multi-compression and multi-collision phenomena that occur within the vertical granular chain. This capability is particularly important for analyzing dynamic systems where multiple interactions occur in rapid succession, as in granular chains. The findings underscore the validity and precision of the proposed viscous contact force model. By accurately simulating both the propagation and reflection of solitary waves, the model provides a reliable tool for studying granular dynamics. This work exemplifies how fluid-inspired contact models can be effectively applied to solid particle interactions, offering new insights into energy transfer and dissipation in granular materials.

7. Conclusions

We introduce a novel viscous fluid damping factor derived from the behavior of incompressible Newtonian fluids based on the Navier-Stokes equations. The dynamic viscosity of the fluid, as incorporated into the new viscous fluid damping factor, represents the energy dissipation occurring during particle impacts. This is analogous to the bulk viscosity of solid bodies during collisions. Once the viscous fluid damping factor is established, a new viscous contact force model is formulated, grounded in the Hertz contact law. Subsequently, a novel coefficient of restitution (CoR) model is developed by applying energy conservation principles during the compression phase of impact. The validity of the CoR model is rigorously tested against experimental data for metallic and nonmetallic materials, affirming the reliability and correctness of the proposed viscous fluid damping factor. Furthermore, the reference solution for the post-impact velocity is determined using the new CoR model and Newton's definition of the CoR. This validation demonstrates that the new viscous contact force model effectively predicts the post-impact motion under varying initial velocities, confirming its robustness and accuracy.

To highlight the advantages of the proposed viscous contact force model over existing models, a systematic comparative analysis is conducted. The CoR values are computed using the new CoR model, and an error analysis is performed to compare these results with the reference solution. The comparison underscores that the new viscous contact model outperforms existing models in accuracy, as it consistently provides results closest to the reference solution. The practical applicability of the new viscous contact model is illustrated through two examples: A bouncing ball scenario and a vertical granular chain. In the case of the bouncing ball, the model successfully reproduces the dynamic response of the ball impacting a rigid plate, showing excellent agreement with experimental data. For the vertical granular chain, the model demonstrates its capability to handle complex phenomena such as multi-collision and multi-compression dynamics, accurately replicating the propagation of solitary waves within the chain.

In summary, this research highlights the reliability and effectiveness of the new viscous contact force model in analyzing impact behaviors. By bridging fluid-based analogies with solid collision dynamics, the study provides a robust framework for exploring complex impact systems. The proposed model not only enhances our understanding of energy dissipation and contact mechanics but also paves the way for future advancements in impact modeling across many applications.

Use of AI tools declaration

The authors declare they have not used Artificial Intelligence (AI) tools in the creation of this article.

Acknowledgments

This work is supported by the National Natural Science Foundation of China (Grant NO.12172004).

Conflict of interest

The authors declare there is no conflict of interest.

References

1. D. Antypov, J. A. Elliott, B. C. Hancock, Effect of particle size on energy dissipation in viscoelastic granular collisions, *Phys. Rev. E: Stat. Nonlinear Soft Matter Phys.*, **84** (2011), 1–8. https://doi.org/10.1103/PhysRevE.84.021303
2. C. Xu, J. Zhu, Experimental and theoretical study on the agglomeration arising from fluidization of cohesive particles—Effects of mechanical vibration, *Chem. Eng. Sci.*, **60** (2005), 6529–6541. https://doi.org/10.1016/j.ces.2005.05.062
3. A. B. Stevens, C. M. Hrenya, Comparison of soft-sphere models to measurements of collision properties during normal impacts, *Powder Technol.*, **154** (2005), 99–109. https://doi.org/10.1016/j.powtec.2005.04.033
4. M. Wojtkowski, J. Pecen, J. Horabik, M. Molenda, Rapeseed impact against a flat surface: Physical testing and DEM simulation with two contact models, *Powder Technol.*, **198** (2010), 61–68. https://doi.org/10.1016/j.powtec.2009.10.015
5. G. S. Ma, X. J. Zheng, The fluctuation property of blown sand particles and the wind-sand flow evolution studied by numerical method, *Eur. Phys. J. E*, **34** (2011). https://doi.org/10.1140/epje/i2011-11054-3
6. M. Motezaker, R. Kolahchi, D. K. Rajak, S. R. Mahmoud, Influences of fiber reinforced polymer layer on the dynamic deflection of concrete pipes containing nanoparticle subjected to earthquake load, *Polym. Compos.*, **42** (2021), 4073–4081. https://doi.org/10.1002/pc.26118
7. R. Kolahchi, H. Hosseini, M. H. Fakhar, R. Taherifar, M. Mahmoudi, A numerical method for magneto-hygro-thermal postbuckling analysis of defective quadrilateral graphene sheets using higher order nonlocal strain gradient theory with different movable boundary conditions, *Comput. Math. Appl.*, **78** (2019), 2018–2034. https://doi.org/10.1016/j.camwa.2019.03.042
8. Y. Feng, S. Huang, Y. Pang, K. Huang, C. Liu, Granular dynamics in auger sampling, *J. Fluid Mech.*, **935** (2022), 1–22. https://doi.org/10.1017/jfm.2022.17
9. W. Kang, Y. Feng, C. Liu, R. Blumenfeld, Archimedes' law explains penetration of solids into granular media, *Nat. Commun.*, **9** (2018), 1–9. https://doi.org/10.1038/s41467-018-03344-3
10. G. Wang, A. Bickerdike, Y. Liu, A. Ferreira, Analytical solution of a microrobot-blood vessel interaction model, *Nonlinear Dyn.*, **2** (2024). https://doi.org/10.1007/s11071-024-10318-2

11. S. Ray, T. Kempe, J. Fröhlich, Efficient modelling of particle collisions using a non-linear viscoelastic contact force, *Int. J. Multiphase Flow*, **76** (2015), 101–110. https://doi.org/10.1016/j.ijmultiphaseflow.2015.06.006
12. Z. Zhao, C. Liu, B. Brogliato, Energy dissipation and dispersion effects in granular media, *Phys. Rev. E: Stat. Nonlinear Soft Matter Phys.*, **78** (2008), 1–13. https://doi.org/10.1103/PhysRevE.78.031307
13. K. Zhang, Dissipative particle dynamics for anti-icing on solid surfaces, *Chem. Phys.*, **568** (2023), 111824. https://doi.org/10.1016/j.chemphys.2023.111824
14. J. He, S. Huang, H. Chen, L. Zhu, C. Guo, X. He, et al., Recent advances in the intensification of triboelectric separation and its application in resource recovery: A review, *Chem. Eng. Process. Process Intensif.*, **185** (2023), 109308. https://doi.org/10.1016/j.cep.2023.109308
15. V. Navarro, E. Tengblad, L. Asensio, A mixed finite element/finite volume formulation for granular bentonite mixtures, *Comput. Geotech.*, **166** (2024), 106018. https://doi.org/10.1016/j.compgeo.2023.106018
16. M. Khan, R. V. More, L. Brandt, A. M. Ardekani, Rheology of dense fiber suspensions: Origin of yield stress, shear thinning, and normal stress differences, *Phys. Rev. Fluids*, **8** (2023), 1–16. https://doi.org/10.1103/PhysRevFluids.8.064306
17. M. R. Brake, P. L. Reu, D. J. VanGoethem, M. V. Bejarano, A. Sumali, Experimental validation of an elastic-plastic contact model, in *ASME International Mechanical Engineering Congress and Exposition*, **54938** (2011), 733–744. https://doi.org/10.1115/imece2011-65736
18. K. R. B. Melo, T. F. de Pádua, G. C. Lopes, A coefficient of restitution model for particle–surface collision of particles with a wide range of mechanical characteristics, *Adv. Powder Technol.*, **32** (2021), 4723–4733. https://doi.org/10.1016/j.apt.2021.10.023
19. G. Wang, W. Jia, F. Cheng, P. Flores, An enhanced contact force model with accurate evaluation of the energy dissipation during contact-impact events in dynamical systems, *Appl. Math. Model.*, **135** (2024), 51–72. https://doi.org/10.1016/j.apm.2024.06.034
20. G. Wang, Z. Niu, F. Cheng, Y. Pan, Analysis of nonphysical attraction force and new coefficient of restitution based on a nonlinear viscoelastic contact model in cohesionless granular system, *Mech. Mach. Theory*, **203** (2024), 105821. https://doi.org/10.1016/j.mechmachtheory.2024.105821
21. S. Ding, Y. Hu, B. Jian, Y. Zhang, R. Xia, G. Hu, A review and comparative analysis of normal contact force models for viscoelastic particles, *Int. J. Impact Eng.*, **189** (2024), 104968. https://doi.org/10.1016/j.ijimpeng.2024.104968
22. B. C. Burman, P. A. Cundall, O. D. L. Strack, A discrete numerical model for granular assemblies, *Geotechnique*, **30** (1979), 331–336. https://doi.org/10.1680/geot.1980.30.3.331
23. B. J. Alder, T. E. Wainwright, Phase transition for a hard sphere system, *J. Chem. Phys.*, **27** (1957), 1208–1209. https://doi.org/10.1063/1.1743957
24. H. Kruggel-Emden, E. Simsek, S. Rickelt, S. Wirtz, V. Scherer, Review and extension of normal force models for the Discrete Element Method, *Powder Technol.*, **171** (2007), 157–173. https://doi.org/10.1016/j.powtec.2006.10.004
25. G. Kuwabara, K. Kono, Restitution coefficient in a collision between two spheres, *Jpn. J. Appl. Phys.*, **26** (1987), 1230–1233.
26. Y. Tsuji, T. Tanaka, T. Ishida, Lagrangian numerical simulation of plug flow of cohesionless particles in a horizontal pipe, *Powder Technol.*, **71** (1992), 239–250. https://doi.org/10.1016/0032-5910(92)88030-L

27. R. Jankowski, Non-linear viscoelastic modelling of earthquake-induced structural pounding, *Earthq. Eng. Struct. Dyn.*, **34** (2005), 595–611. https://doi.org/10.1002/eqe.434
28. T. Schwager, T. Pöschel, Coefficient of normal restitution of viscous particles and cooling rate of granular gases, *Phys. Rev. E*, **57** (1998), 650–654. https://doi.org/10.1103/PhysRevE.57.650
29. J. Lee, H. J. Herrmann, Angle of repose and angle of marginal stability: Molecular dynamics of granular particles, *J. Phys. A: Math. Gen.*, **26** (1993), 373–383. https://doi.org/10.1088/0305-4470/26/2/021
30. G. Ristow, Simulating granular flow with molecular dynamics, *J. Phys. I*, **2** (1992), 649–662.
31. C. Spitas, M. S. Dwaikat, V. Spitas, Effect of the elastic hysteresis term formulation and response to non-harmonic periodic excitations of a non-linear SDOF dynamical model with weak frequency-dependency in the time domain, *Proc. Inst. Mech. Eng., Part C: J. Mech. Eng. Sci.*, **235** (2021), 4637–4647. https://doi.org/10.1177/09544062211018252
32. C. Spitas, M. M. S. Dwaikat, V. Spitas, Non-linear modelling of elastic hysteretic damping in the time domain, *Arch. Mech.*, **72** (2020), 323–353. https://doi.org/10.24423/aom.3536
33. J. S. Marshall, Viscous damping force during head-on collision of two spherical particles, *Phys. Fluids*, **23** (2011), 1–10. https://doi.org/10.1063/1.3546094
34. M. Utsumi, Slosh damping caused by friction work due to contact angle hysteresis, *AIAA J.*, **55** (2017), 265–273. https://doi.org/10.2514/1.J055238
35. X. Shi, A. A. Polycarpou, Measurement and modeling of normal contact stiffness and contact damping at the meso scale, *J. Vib. Acoust.*, **127** (2005), 52–60. https://doi.org/10.1115/1.1857920
36. L. Peng, Z. Gao, Z. Ban, F. Gao, W. Fu, Dynamic tangential contact stiffness and damping model of the solid–liquid interface, *Machines*, **10** (2022). https://doi.org/10.3390/machines10090804
37. W. Zhang, C. Zhang, L. Su, Y. Zheng, X. Du, Experimental study on the dynamic performance of a winding rope fluid viscous damper, *Eng. Struct.*, **281** (2023), 115786. https://doi.org/10.1016/j.engstruct.2023.115786
38. W. Zhang, K. Turner, Frequency dependent fluid damping of micro/nano flexural resonators: Experiment, model and analysis, *Sens. Actuators, A*, **134** (2007), 594–599. https://doi.org/10.1016/j.sna.2006.06.010
39. E. Alizadeh, F. Bertrand, J. Chaouki, Development of a granular normal contact force model based on a non-Newtonian liquid filled dashpot, *Powder Technol.*, **237** (2013), 202–212. https://doi.org/10.1016/j.powtec.2013.01.027
40. Y. Ye, Y. Zeng, A size-dependent viscoelastic normal contact model for particle collision, *Int. J. Impact Eng.*, **106** (2017), 120–132. https://doi.org/10.1016/j.ijimpeng.2017.03.020
41. M. Poursina, P. E. Nikravesh, Characterization of the optimal damping coefficient in the continuous contact model, *J. Comput. Nonlinear Dyn.*, **15** (2020). https://doi.org/10.1115/1.4047136
42. T. Schwager, T. Pöschel, Coefficient of restitution for viscoelastic spheres: The effect of delayed recovery, *Phys. Rev. E: Stat. Nonlinear Soft Matter Phys.*, **78** (2008), 1–12. https://doi.org/10.1103/PhysRevE.78.051304
43. S. Ji, H. H. Shen, Effect of contact force models on granular flow dynamics, *J. Eng. Mech.*, **132** (2006), 1252–1259. https://doi.org/10.1061/(asce)0733-9399(2006)132:11(1252)
44. N. V. Brilliantov, N. Albers, F. Spahn, T. Pöschel, Collision dynamics of granular particles with adhesion, *Phys. Rev. E: Stat. Nonlinear Soft Matter Phys.*, **76** (2007), 1–12. https://doi.org/10.1103/PhysRevE.76.051302

45. T. Schwager, T. Pöschel, Coefficient of normal restitution of viscous particles and cooling rate of granular gases, *Phys. Rev. E: Stat. Phys. Plasmas Fluids Relat. Interdiscip. Top.*, **57** (1998), 650–654. https://doi.org/10.1103/PhysRevE.57.650.
46. Y. Liu, X. Yu, General formulation of drag force on assemblage of spherical particles in fluids: A critical review and a new empirical formula, *Phys. Fluids*, **34** (2022). https://doi.org/10.1063/5.0096069
47. P. Flores, M. MacHado, M. T. Silva, J. M. Martins, On the continuous contact force models for soft materials in multibody dynamics, *Multibody Syst. Dyn.*, **25** (2011), 357–375. https://doi.org/10.1007/s11044-010-9237-4
48. R. L. Jackson, I. Green, D. B. Marghitu, Predicting the coefficient of restitution of impacting elastic-perfectly plastic spheres, *Nonlinear Dyn.*, **60** (2010), 217–229. https://doi.org/10.1007/s11071-009-9591-z
49. J. Horabik, M. Beczek, R. Mazur, P. Parafiniuk, M. Ryżak, M. Molenda, Determination of the restitution coefficient of seeds and coefficients of visco-elastic Hertz contact models for DEM simulations, *Biosyst. Eng.*, **161** (2017), 106–119. https://doi.org/10.1016/j.biosystemseng.2017.06.009
50. M. J. Lichtensteiger, *Impact Analysis of Viscoelastic Spheres, Fruits and Vegetables With Rigid, Plane Surfaces*, The Ohio State University, 1982.
51. P. Gondret, M. Lance, L. Petit, Bouncing motion of spherical particles in fluids, *Phys. Fluids*, **14** (2002), 643–652. https://doi.org/10.1063/1.1427920
52. Y. Feng, W. Kang, D. Ma, C. Liu, Multiple impacts and multiple-compression process in the dynamics of granular chains, *J. Comput. Nonlinear Dyn.*, **14** (2019). https://doi.org/10.1115/1.4044584
53. C. Daraio, V. F. Nesterenko, E. B. Herbold, S. Jin, Tunability of solitary wave properties in one-dimensional strongly nonlinear phononic crystals, *Phys. Rev. E: Stat. Nonlinear Soft Matter Phys.*, **73** (2006), 1–10. https://doi.org/10.1103/PhysRevE.73.026610
54. C. Daraio, V. F. Nesterenko, E. B. Herbold, S. Jin, Energy trapping and shock disintegration in a composite granular medium, *Phys. Rev. Lett.*, **96** (2006), 1–4. https://doi.org/10.1103/PhysRevLett.96.058002

AIMS Press